



Cardiac amyloidosis detection by early bisphosphonate (99mTc-HMDP) scintigraphy

M. F. Santarelli, PhD,^{a,b} D. Genovesi, MD,^b V. Positano, MSc,^b R. Di Sarlo, MSc,^c M. Scipioni, PhD,^{a,d} A. Giorgetti, MD,^b L. Landini, Prof,^{b,c} and P. Marzullo, MD^b

^a CNR Institute of Clinical Physiology, CNR Research Area, Pisa, Italy

^b Fondazione Toscana “G. Monasterio”, CNR Research Area, Pisa, Italy

^c Dipartimento di Ingegneria dell’Informazione: DII, Pisa University, Pisa, Italy

^d Athinoula A. Martinos Center for Biomedical Imaging, Massachusetts General Hospital and Harvard Medical School, Boston, MA

Received Feb 26, 2020; accepted Jun 9, 2020

doi:10.1007/s12350-020-02239-5

Objective. To determine one or more indexes able to detect the presence of cardiac amyloidosis (CA) from planar scintigraphy images after injection of 99mTc-HMDP tracer and to identify the earliest acquisition time able to ensure an accurate diagnosis of amyloid transthyretin CA.

Methods and Results. A total of 38 patients were included: 18 subjects with a final diagnosis of ATTR-CA and 20 controls. Dynamic planar images of the anterior thorax were acquired, starting at intravenous injection of ≈ 700 MBq of 99mTc-HMDP. From time/activity curves (TAC) of regions of interest such as heart, vascular region, right ribcage, and soft tissues, several indices were considered. From the analysis, it resulted that both $TAC_{Heart/Bone}(t)$ and $RI_{heart-bone}(t)$, for $t > 6$ minutes, well distinguish ATTR-CA patients from controls subjects. This is confirmed by the area under curves (AUC) analysis giving AUC values ≈ 0.9 at $t \approx 6$ minutes and $AUC \approx 1$ for $t > 10$ minutes.

Conclusions. The method proposed allows determining the presence of ATTR-CA, in an inexpensive manner both in terms of examination costs and time spent. (J Nucl Cardiol 2022;29:307–18.)

Key Words: Cardiac amyloidosis • Amyloid transthyretin (ATTR) • Early 99mTc-HMDP scintigraphy • Dynamic time-activity curves • Retention index

Abbreviations		nRMSE	Normalized root mean square error
AL	Immunoglobulin light-chain derived amyloidosis	RI	Retention index
ATTR	Transthyretin derived amyloidosis	ROI	Region of interest
AUC	Area under curves	SEM	Standard error measure
CA	Cardiac amyloidosis	TAC	Time/activity curve
HMDP	Hydroxymethylene diphosphonate		

See related editorial, pp. 319–322

Electronic supplementary material The online version of this article (<https://doi.org/10.1007/s12350-020-02239-5>) contains supplementary material, which is available to authorized users.

The authors of this article have provided a PowerPoint file, available for download at SpringerLink, which summarizes the contents of the paper and is free for re-use at meetings and presentations. Search for the article DOI on SpringerLink.com.

All editorial decisions for this article, including selection of reviewers and the final decision, were made by guest editor Stephan Nekolla, MD.

Reprint requests: M. F. Santarelli, PhD, CNR Institute of Clinical Physiology, CNR Research Area, Via Moruzzi 1, 56124 Pisa, Italy; mariafilomena.santarelli@cnr.it

1071-3581/\$34.00

Copyright © 2020 American Society of Nuclear Cardiology.

INTRODUCTION

Cardiac amyloidosis (CA) is a disorder characterized by the extracellular deposition of insoluble protein-derived fibrils within the myocardium. The main subtypes of cardiac amyloidosis are the immunoglobulin light-chain derived amyloidosis (AL) and the transthyretin derived amyloidosis (ATTR). Cardiac involvement of amyloidosis leads to a progressive dysfunction up to early death due to heart failure (HF) and arrhythmias.¹

Unfortunately, the diagnosis of CA is frequently delayed,¹ mainly because of the similarities between CA and other mimicking conditions such as hypertrophic cardiomyopathy; consequently, appropriate therapies are also delayed. Histological assessment is often required in order to identify the specific subtype of CA, in particular when a monoclonal component in serum or in urine is present.² Subcutaneous fat, salivary gland, or rectal mucosa biopsies often yield a reliable diagnosis of systemic AL³ and ATTR amyloidosis⁴; however, frequently, a more invasive and risky endomyocardial biopsy (EMB) might also be required to confirm the diagnosis of cardiac involvement of the disease, even though this approach is burdened by greater complications. Therefore, an alternative accurate, non-invasive, and reproducible method to diagnose CA is necessary.

Recently, imaging techniques, as echography,^{5,6} cardiac magnetic resonance⁷⁻⁹ or molecular imaging^{1,10-12} are used in clinical practice for the diagnosis of CA.

It has been widely demonstrated that molecular imaging after bone-tracer injection, combined with specific biomarkers, has the capacity to identify ATTR-CA. Among the bisphosphate derivative tracers labeled with the isotope ^{99m}Tc, the most used for CA diagnosis are ^{99m}Tc-pyrophosphate (^{99m}Tc-PYP), ^{99m}Tc-3,3'-diphosphono-1,2-propanodicarboxylic acid (^{99m}Tc-DPD), and ^{99m}Tc-hydroxymethylene diphosphonate (^{99m}Tc-HMDP).¹³ Such tracers can be used in planar imaging or/and in single-photon emission computed tomography (SPECT)¹⁴⁻¹⁷

Planar anterior images of the thorax are usually acquired 1 hour after the injection, or more frequently after 3 hours, thus forcing patients to stay in the laboratory while waiting. Galat et al.¹⁸ demonstrated that early phase (10 min) ^{99m}Tc-HMDP scintigraphy is able to predict late-phase (3 hours) finding. However, the shortest acquisition time that allows identifying CA has not been validated yet.¹⁹

Images interpretation is usually performed by means of a semi-quantitative grading score,²⁰ or by visual assessment using a qualitative score.²¹⁻²³

The main objective of the present study is to determine one or more quantitative parameters able to

detect the presence of CA from early bone-seeking agent scintigraphy and to identify the earliest acquisition time able to ensure an accurate diagnosis of ATTR-CA. Since CA patients are often debilitated and fragile, the possibility to obtain a correct diagnosis from an early phase acquisition would greatly reduce the waiting time, thus increasing the efficacy in terms of comfort and acceptance by patients.

Moreover, given the wide availability and cost-effectiveness of the standard gamma-camera equipment required, the method proposed in this work could provide a reliable, and yet affordable, approach to the diagnosis and characterization of CA.

MATERIALS AND METHODS

Subjects and Study Design

A total of 38 patients were included in this retrospective study: all patients underwent to clinical examination, blood and urine sampling for dosage of specific serum and urinary biomarkers (terminal N fraction of pro-brain natriuretic peptide, high sensitivity troponin T, immunoglobulin light chains in serum and / or urine), genetic evaluation for transthyretin gene mutations, electrocardiogram, echocardiography, ^{99m}Tc-Hydroxymethylene diphosphonate scintigraphy, cardiac magnetic resonance and histological evaluation to assess amyloid deposition, according to the most recent indications^{2,18,24} patients received a final diagnosis of ATTR-CA, while 20 patients received an alternative diagnosis (10 hypertensive cardiomyopathies, 8 hypertrophic cardiomyopathies secondary to aortic stenosis and 2 primary hypertrophic cardiomyopathies). None of the patients included in the study had a monoclonal component in serum and/or in urine. Patients with ischemic heart disease, chronic liver disease or severe renal failure were excluded from the study. Patients who received an alternative diagnosis to CA were considered as control subjects in this study. A summary description of the overall population and the two subgroups of patients are shown in Table 1.

The study was approved by the institutional ethics committee and by the AIFA (Agenzia Italiana del Farmaco) committee; all subjects signed an informed consent form. The study complied with the Declaration of Helsinki.

Bisphosphonate (^{99m}Tc-HMDP) Scintigraphy and Dynamic Time-Activity Curves Generation

Each patient underwent to scintigraphic scan starting at intravenous injection of ≈ 700 MBq of ^{99m}Tc-

HMDP (70 MBq/cc with an infusion rate of 1 cc/s followed by a 10 cc flush of saline solution), providing an expected radiation dose of ≈ 5 mSv per patient. Dynamic planar images with a resolution of 128×128 pixels of the anterior thorax were acquired from the radiotracer injection up to 1050 seconds (17.5 minutes), with the following non-uniform time scheme: 240×0.5 , 1×30 , 12×60 , 1×180 seconds. Moreover, three late static planar images of the anterior thorax were acquired for 5 minutes, respectively 1, 2 and 3 hours after tracer injection using the same resolution mentioned above. Images were acquired with a dual-headed gamma-camera equipped with LEHR collimators (Millennium MG–GE Healthcare, Haifa–Israel). Cardiac uptake of ^{99m}Tc -HMDP was assessed on the late static planar images according to the grading scale proposed by Perugini et al.²⁰: grade 0 = absent cardiac uptake; grade 1 = mild uptake, less than bone; grade 2 = moderate uptake, equal to bone; and grade 3 = high uptake, greater than bone.

All the 20 subjects considered as “control group” had a cardiac uptake of grade 0 while all the 18 patients with CA presented significant cardiac uptake of the radiotracer; in particular none of the patients presented a cardiac uptake of grade 1, while 7 and 11 patients had a cardiac uptake of grade 2 and 3 respectively.

Time/activity curves (TAC) were obtained from the dynamic planar images by manually drawing a region of interest (ROI) over the frame with the best visualization of the specific anatomical structure to be measured and then replicating it over the whole frame-set.

ROIs were selected by a nuclear physician (DG) with more than 10 years of experience in cardiac nuclear medicine. In order to evaluate the intra-observer variability, he repeated the analysis a second time, about a week after the first one. Then, for evaluating the inter-observer variability, a second nuclear physician (AG, > 10 years experience), further performed the measurements. Both observers were blinded to each other’s results.

As an example, in Figure 1 scintigraphic images of an ATTR-CA patient, with over imposed selected ROIs are shown. In particular, image in Figure 1A was acquired at about 1 minute (60.25 seconds), i.e., in the vascular phase of the tracer; image in Figure 1B was acquired at 5 minutes and half (330 seconds), i.e., in the early phase; image in Figure 1C was acquired at 1 hours after injection. Note that, in the early phase image, the presence of the tracer in the heart is already evident.

Radioactive counts in each ROI were then measured on dynamic images in order to obtain specific TACs of the heart ($\text{TAC}_{\text{heart}}$), the vascular region ($\text{TAC}_{\text{blood}}$), the right ribcage (TAC_{bone}), and soft tissues of the axillary

Table 1. Clinical, scintigraphic, echocardiographic and biochemical characteristics of the examined patients and of the two scintigraphic subpopulations (i.e., controls and ATTR-CA patients)

	Overall	Positive scintigraphy	Negative scintigraphy	P
Age (year)	82.1 \pm 6.3	81.0 \pm 7.8	82.9 \pm 4.9	NS
Sex(M/F)	58% 42%	89% 11%	30% 70%	< .01
Perugini score (0/2/3)	53% 18% 29%	0% 39%	100% 0% 0%	< .01
NYHA (I-II/III-IV)	74% 26%	62% 38%	83% 17%	NS
E/E'	14.0 (13.0–20.0)	20.0 (13.5–23.0)	13.0 (12.0–13.8)	.04
E/A (cm/sec)	1.2 (0.7–2.2)	2.0 (0.8–3.0)	0.8 (0.6–1.4)	NS
EDV (ml)	104.8 \pm 30.3	101.6 \pm 24.4	107.6 \pm 35.3	NS
ESV (ml)	49.7 \pm 23.1	51.7 \pm 16.9	48.0 \pm 27.9	NS
EF %	54.3 \pm 12.6	49.3 \pm 10.9	58.4 \pm 12.8	NS
Septal wall thickness (mm)	16.5 \pm 3.8	18.7 \pm 3.8	14.5 \pm 2.6	< .01
Posterior wall thickness (mm)	13.7 \pm 3.2	15.8 \pm 3.0	11.9 \pm 2.0	< .01
LVMi (g/m ²)	150.0 (132.6–172.9)	177.0 (148.0–230.7)	126.0 (105.8–154.5)	< .01
Nt-proBNP (ng/L)	1550.0 (812.9–4304.8)	4020.5 (1744.7–10596.5)	782.5 (359.6–2866.8)	NS
HS TnT (ng/L)	37.0 (20.1–61.3)	70.8 (39.6–147.9)	20.0 (14.3–42.2)	< .01

Variables with normal distribution were presented as mean \pm SD, whereas those with non-normal distribution were presented as median (95% confidence interval); categorical variables were shown as percentages. Differences among groups were tested by one-way analysis of variance or by Chi-square test, as appropriate

area (TAC_{back}) considered as background. Each TAC was normalized by the injected dose, the tracer decay, and the ROI area. In Figure 2, as an example, the dynamic TAC_{heart} , TAC_{blood} , TAC_{bone} , and TAC_{back} relevant to a control subject (in A) and a patient (in B) are shown. In the figure, the activity values (in a.u.) from late images, i.e., at 60 minutes, are also shown in the inner boxes. In

Figure 2C and D, whole body scans of the two subjects, acquired three hours after the injection, are shown.

Indices Used for the Analysis

The following indices were considered to assess whether it is possible to reliably detect the presence of

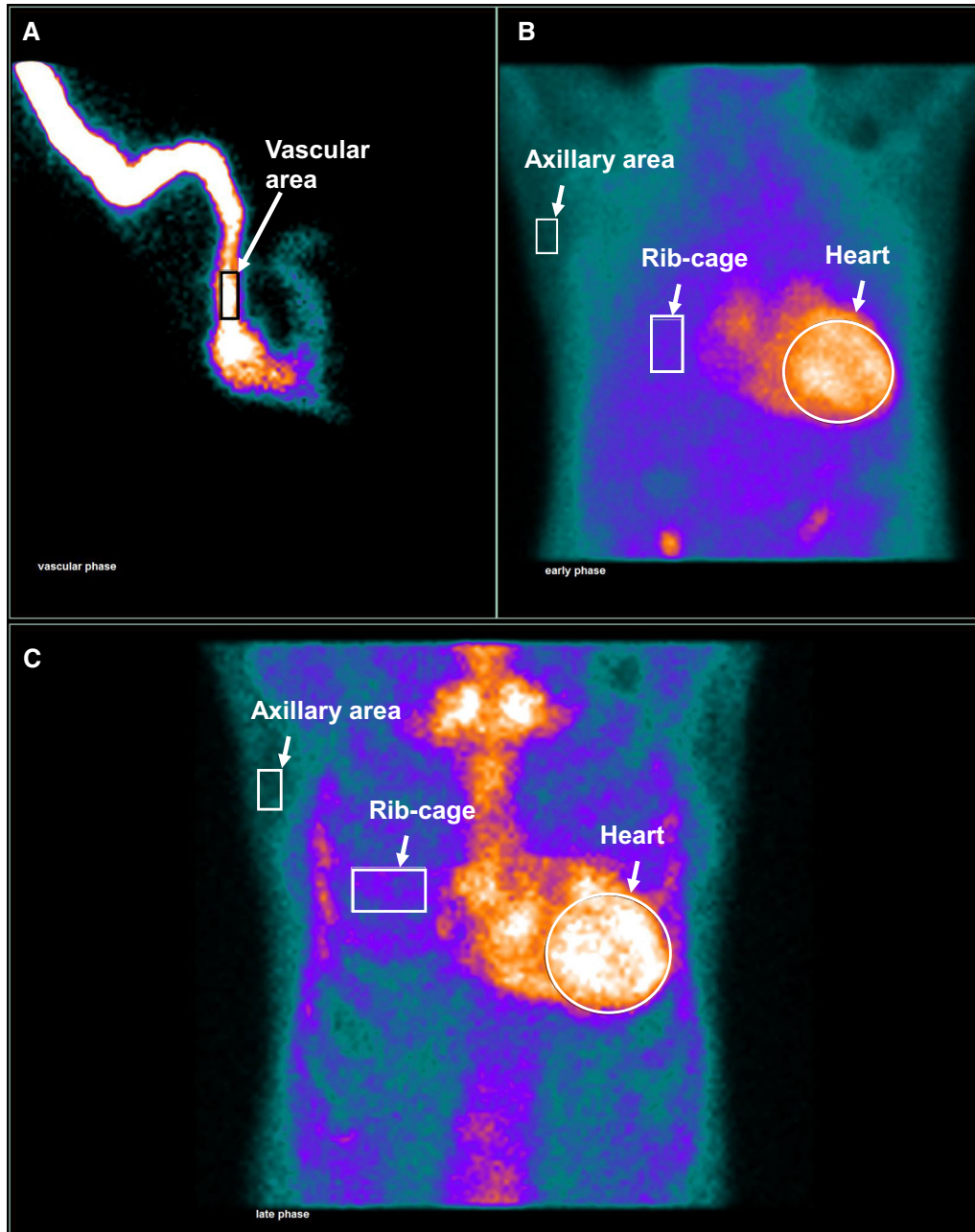


Figure 1. Scintigraphy images with over imposed selected ROIs. **A** Image acquired at 60.25 second (vascular phase), **B** image acquired at 330 seconds (early phase), **C** image acquired at 1 hour after injection. In the early phase image, the presence of the tracer in the heart is already evident.

CA from early images, acquired a few minutes after tracer injection.

Time-activity curves In addition to TAC_{heart} , TAC_{blood} , TAC_{bone} , and TAC_{back} extracted as previously described, the following curves were also computed by properly combining pairs of such curves:

$$TAC_{\text{heart/back}}(t) = TAC_{\text{heart}}(t)/TAC_{\text{back}}(t)$$

$$TAC_{\text{heart-back}}(t) = TAC_{\text{heart}}(t) - TAC_{\text{back}}(t)$$

$$TAC_{\text{heart/bone}}(t) = TAC_{\text{heart}}(t)/TAC_{\text{bone}}(t)$$

$$TAC_{\text{heart-bone}}(t) = TAC_{\text{heart}}(t) - TAC_{\text{bone}}(t)$$

For each TAC, we treated each time point $TAC(t)$ as a separate index, ending up with 283 indices for each curve.

Retention values Retention index is often used when images acquired at different times are available.^{25,26} In our case, having dynamic images available, it was possible to determine the retention value of the tracer over time ($RI_{\text{ROI}}(t)$, where ROI is either ‘heart’, or ‘bone’, or ‘background’), as follows:

$$RI_{\text{ROI}}(t) = TAC_{\text{ROI}}(t)/\int_0^t TAC_{\text{blood}}(t')dt'$$

Furthermore, combinations of Retention values from multiple ROIs were also considered, as:

$$RI_{\text{heart/bone}}(t) = RI_{\text{heart}}(t)/RI_{\text{bone}}(t)$$

$$RI_{\text{heart-bone}}(t) = RI_{\text{heart}}(t) - RI_{\text{bone}}(t)$$

$$RI_{\text{heart/back}}(t) = RI_{\text{heart}}(t)/RI_{\text{back}}(t)$$

As for the indices associated with each $TAC_{\text{ROI}}(t)$, also for each $RI_{\text{ROI}}(t)$, we have as many indices as there are time points on the RI curve.

Intra-Inter-observer Variability Analysis

Intra- and inter-observer variabilities were evaluated in two phases of the study, (i) the variability of the TACs extracted from the ROIs can strongly influence the subsequent stages of the analysis; for this reason it was measured by the normalized root mean square error (nRMSE); (ii) one of the last steps of the analysis includes the evaluation of the threshold time for each index previously described, i.e., the time after which the index significantly differentiates the two groups

(Controls and CA Patients); it was measured by the standard error measure (SEM).

In particular, the nRMSE for a ROI was evaluated according to the following equation:

$$nRMSE_{\text{ROI}} = \text{mean}_{\text{subj}} \left(\sqrt{\frac{\sum_{t=1}^N (x_t - y_t)^2 / N}{\hat{x}}} \right) * 100$$

where x and y are the TACs derived from the ROIs selected (at different times for the intra-observer study, and from different operators for the inter-observer study); \hat{x} is the mean of the TAC x ; N is the number of time points of the curve; $\text{mean}_{\text{subj}}(.)$ stands for the mean over all the subjects analyzed. nRMSE evaluation was repeated for each selected ROI.

The SEM was given by²⁷:

$$SEM = \sqrt{\frac{(\text{Tresh_time}_1 - \text{Tresh_time}_2)^2 / 2}{(\text{Tresh_time}_1 + \text{Tresh_time}_2) / 2}}$$

where Tresh_time is the threshold time obtained at the final stage of data analysis; 1 and 2 relate to the results obtained from the measurements performed by the operator in two different times (for intra-observer variability analysis) or performed by the two operators (for inter-observer analysis).

SEM evaluation was repeated for each index under consideration in the study.

Statistical Analysis Methods

Continuous variables are expressed as mean \pm standard deviation or median and range (i.e., 1st and 3rd quartiles), as appropriate.

The parametric hypothesis test of normality of the variables was evaluated according to the Shapiro-Willis normality test. When the indices evaluated do not follow Normal Distribution the Mann-Whitney test was used for comparison between two group samples. A 2-tailed P value $< .05$ was considered significant.

Statistical analysis was performed using MATLAB Statistics and Machine Learning ToolboxTM (version 2018b).

RESULTS

From the Shapiro-Willis normality test, it resulted that the indices evaluated for the analysis were not Gaussian, so the following resulting data were shown as median and 1st and 3rd quartiles.

In Figure 3 the median and quartiles of $TAC_{\text{ROI}}(t)$ are shown; ROIs are: heart in **A**, heart/background in **B**,

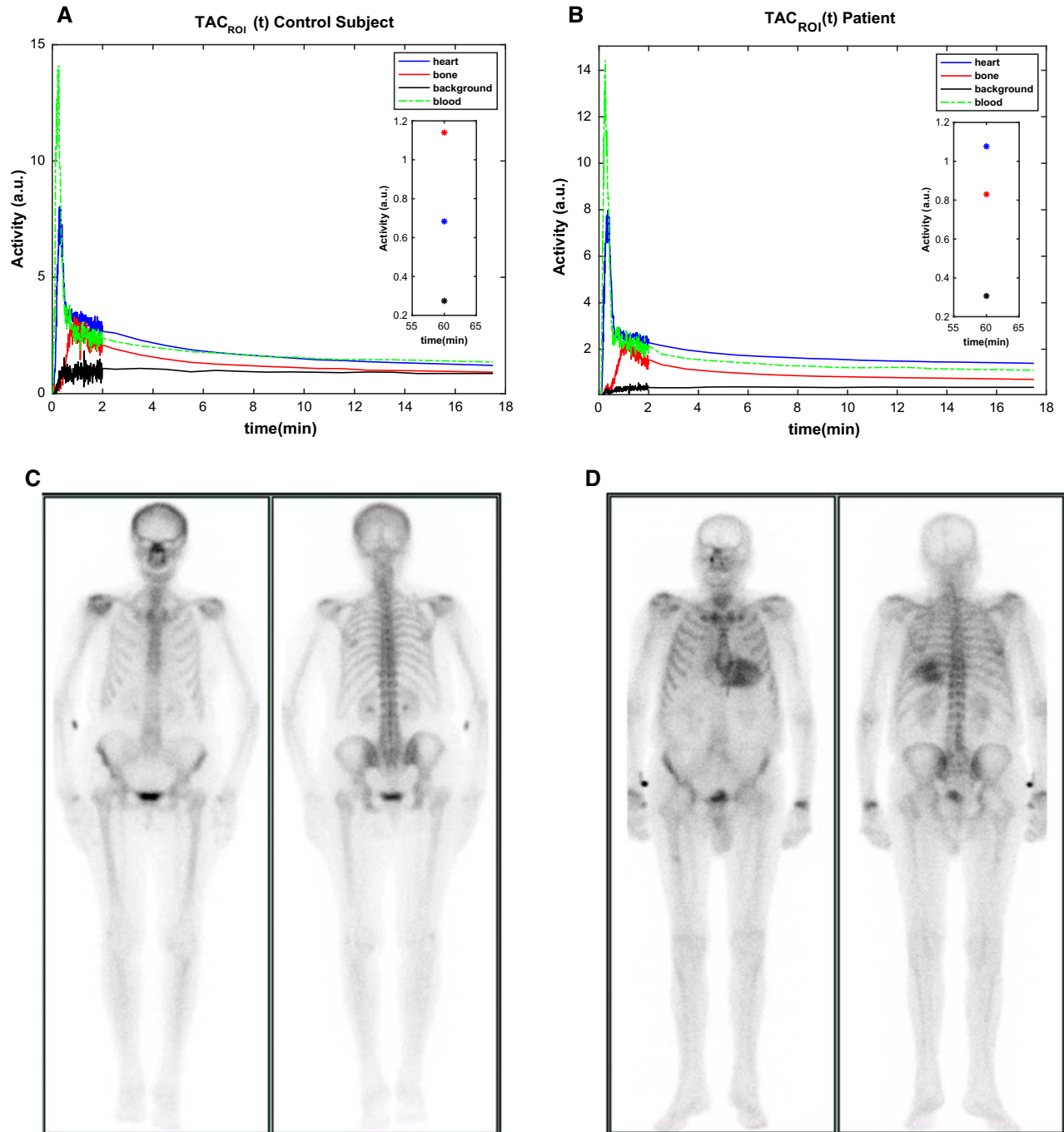


Figure 2. Examples of selected ROIs and time-activity curves (TAC), and whole-body late (3 hours) scans; **A** TACs derived from a Control subject, **B** TACs derived from a CA patient. The inner boxes show the activity at 60 minutes, **C** whole-body late scan of patient in **A**, **D** whole-body late scan of patient in **B**.

heart-background in **C**, heart/bone in **D**, heart–bone in **E**.

In each graph, the red continuous line is related to the index value for CA Patient data, the blue line is

related to the index value for Control subjects data. Making a qualitative consideration, in each graph it is quite clear that, from a certain time value onwards, the two continuous lines distance themselves from each

other, that is, the index distinguishes the two groups of subjects. Even the shaded bands (representing the quartiles limits) of the same color of the continuous lines, especially from a certain value of time onwards, move away from each other, and this is more evident for some indices such as $TAC_{Heart/Bone}(t)$ (Figure 3D) and $TAC_{Heart-Bone}(t)$ (Figure 3E).

As a more quantitative result of the analysis, in each graph of Figure 3 the Mann–Whitney test result is shown, by means of a black dotted line (see also Table 2).

In Figure 4 the median and quartiles of $RI_{ROI}(t)$ are shown; ROIs are: heart in **A**, heart/background in **B**, heart-background in **C**, heart/bone in **D**, heart–bone in **E**.

Similarly to the results of Figure 3, also from the data shown in Figure 4 it is possible to make the consideration that from a certain time value onwards the

two lines move away from each other: starting from that time value the index can distinguish the data of CA Patients from those of Control subjects. This is very evident for the $RI_{Heart-Bone}(t)$ index (Figure 4E)

Also in Figure 4 the most quantitative result obtained by the Mann–Whitney test is shown in each graph with a black dotted line.

Table 2 shows the results of the Mann–Whitney test for the comparison between Control subjects and CA Patients. In the table, for each index considered in the analysis, the threshold time and the relevant *P* value are shown. The resulting threshold time is the minimum time from tracer injection, from which the index value significantly distinguishes the two groups of subjects.

The Area under the curve (AUC) from the Receiver Operating Characteristic (ROC) evaluated for each index, at each time, is shown in Figure 5.

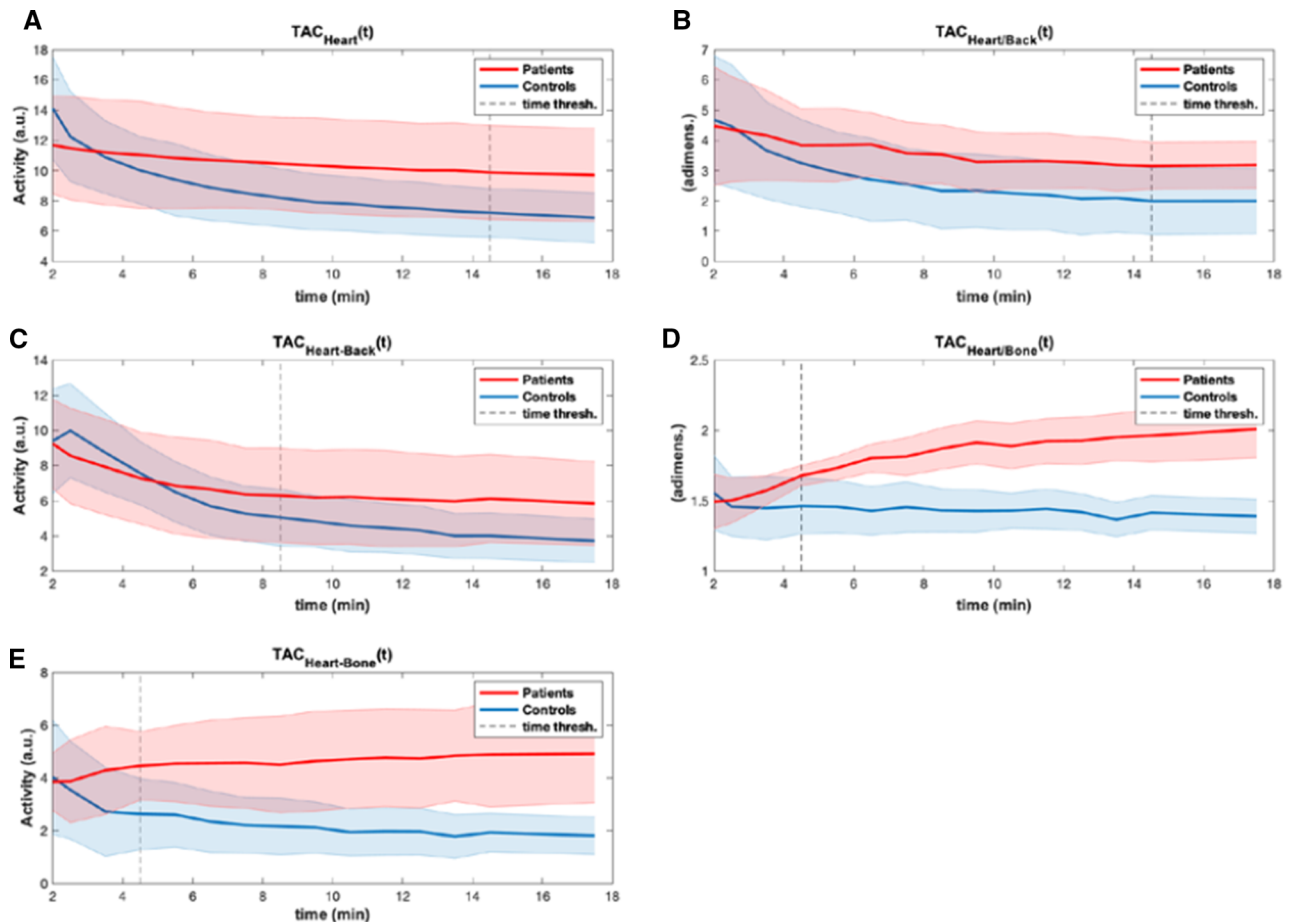


Figure 3. Median and 1st and 3rd quartiles of $TAC_{ROI}(t)$ from Controls and CA amyloidosis Patients. **A** Heart, **B**: heart/background, **C** heart-background, **D** heart/bone, **E** heart–bone. Dotted lines represent the time threshold beyond which the two groups are significantly different, according to the Mann-Whitney test.

The maximum accuracy value was 97.4%, obtained with the $RI_{\text{Heart-bone}}(t)$ index.

Intra-Inter-observer Variability Analysis

In Table 3 the mean \pm standard deviation nRMSE values from the TACs derived from the selected ROIs are shown. As a global view of the results, we considered the mean of $nRMSE_{\text{ROI}}$ over all the ROIs in the intra-observer measurement that resulted equal to 3.68% and the mean $nRMSE_{\text{ROI}}$ in the inter-observer measurements resulted equal to 6.60%

The SEM from the measures of threshold time for each index, resulted to have a minimum value of 0% and maximum value of 0.20% (mean 0.04%) in both intra- and inter-observer variabilities.

DISCUSSION

In the clinical practice, when CA is suspected, bone scintigraphy is often required in order to obtain a non-invasive diagnosis of ATTR-CA. Usually, the examination consists of acquiring a static image one or 3 hours after the tracer administration.^{28,29}

Interpretation of scintigraphy with bisphosphate derivative tracers is usually performed by visual analysis, or/and quantitative or semi-quantitative analysis. As far as visual analysis, uptake is typically categorized as absent, local, or diffuse.²² ATTR cardiac amyloidosis usually presents as diffuse uptake on late acquired images. One semi-quantitative evaluation method often used in ATTR-CA diagnosis consists of a grading system that relies on visual comparison of the myocardial and rib uptake on images acquired 3 hours after tracer injection.²⁰ Quantitative analysis methods consist

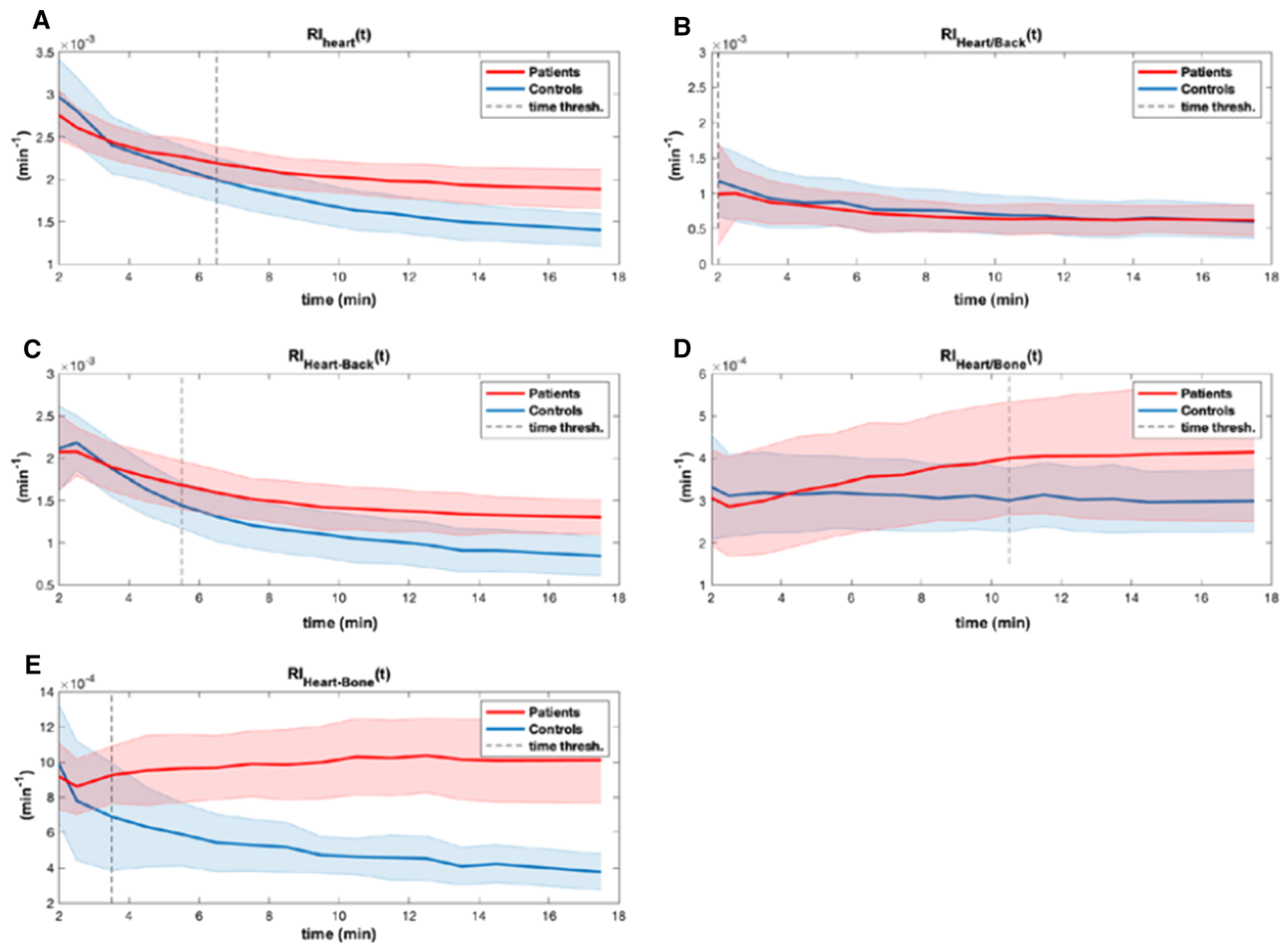


Figure 4. Median and 1st and 3rd quartiles of $RI_{\text{ROI}}(t)$ from Controls and CA amyloidosis Patients. **A** Heart, **B** heart/background, **C** heart-background, **D** heart/bone, **E** heart-bone. Dotted lines represent the time threshold beyond which the two groups are significantly different, according to the Mann-Whitney test.

Table 2. Mann-Whitney test results; comparison between Control subjects and CA Patients group samples

Index	Threshold time (min)	P value
TAC _{Heart} (t)	14.5	< .05
TAC _{Heart/Back} (t)	14.5	< .05
TAC _{Heart-Back} (t)	8.5	< .05
TAC _{Heart/Bone} (t)	4.5	< .05
TAC _{Heart-Bone} (t)	4.5	< .05
RI _{Heart} (t)	6.5	< .05
RI _{Heart/Back} (t)	2	.68
RI _{Heart-Back} (t)	5.5	< .05
RI _{Heart/Bone} (t)	10.5	< .05
RI _{Heart-Bone} (t)	3.5	< .05

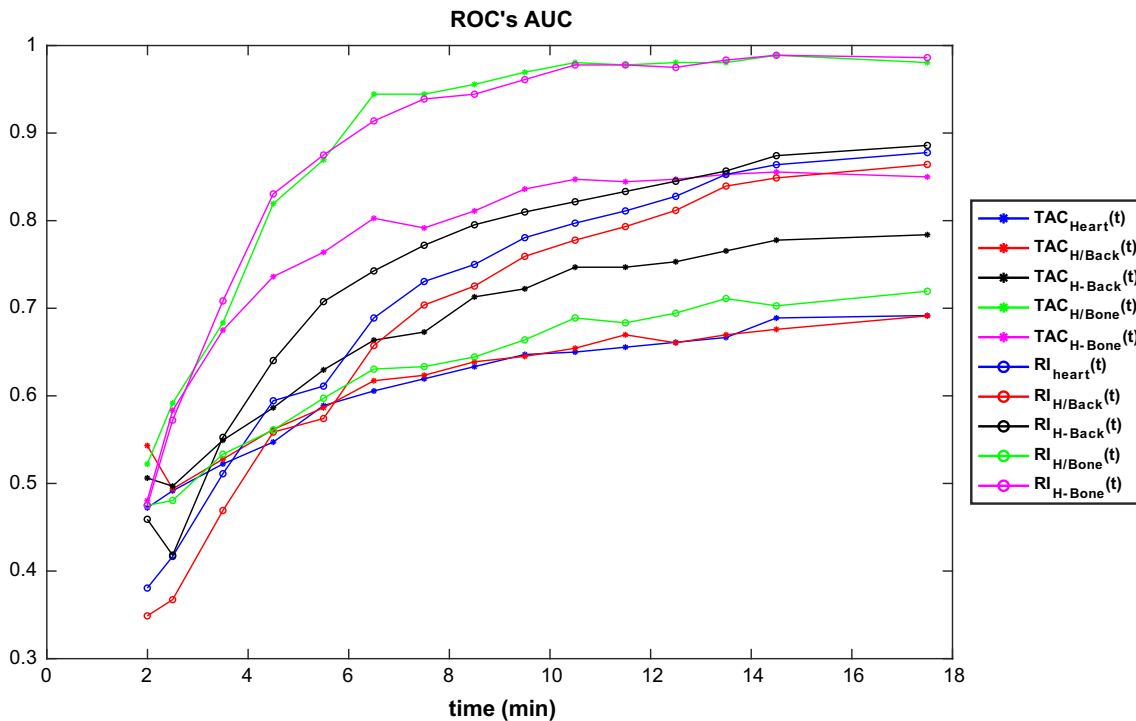


Figure 5. AUC from ROC evaluated for each index at each time value.

of a set of indices derived from the acquired images, such as heart/contralateral thorax count ratio,^{22,30,31} heart tracer retention,^{13,18} whole-body tracer retention,^{13,32,33} heart to whole-body uptake ratio,^{13,32,33} heart to skull uptake ratio.³³ In Gallini et al.,²³ several indices for the detection of CA deposits were reported, but they were only evaluated on static images acquired 150 minutes after tracer injection. Indices involving

retention need an acquisition at about 5 minutes after injection followed by a late acquisition, usually 1 or 3 hours after injection.

In this study, we explored the possibility of achieving an accurate diagnosis of ATTR-CA from images acquired shortly after the injection, and to estimate the minimum acquisition time to have a reliable result. This analysis was carried out using specific indices extracted

from dynamic scintigraphy images acquired starting from the injection of 99mTc-HMDP.

Indices were obtained directly from the heart TAC curves, suitably normalized with respect to other ROIs (bone or background), or from the retention values of the tracer in the heart, suitably normalized. While the indices extracted directly from the TAC curves use only static images acquired in a short interval of time, those derived from retention require longer acquisitions, that is, from a start time (usually 2 to 3 minutes after the injection) and for a few minutes. From the results shown in Figures 3, 4 and 5 and in Table 2, however, these times result to be very short: less than 10 to 15 minutes.

Results shown in Figure 3 are relevant to the analysis of $TAC_{ROI}(t)$ indices, where ROIs are, respectively, heart, heart/background, heart–background, heart/bone, heart–bone. From the figure, it should be noted that the $TAC_{Heart/Bone}(t)$, for $t > 6$ minutes, well distinguish ATTR-CA patients from controls, also considering the quartiles values; for this index, according to the Mann–Whitney test (Table 2) the time $t = 4.5$ minutes results to be the minimum time for significantly distinguishing the two groups.

From the results shown in Figure 4, relevant to the analysis of $RI_{ROI}(t)$ indices, it can be affirmed that $RI_{heart-bone}(t)$, for $t > 6$ minutes well distinguish ATTR-CA Patients group from Control subjects, considering also the indices values falling within 1st and 3rd quartiles; moreover, from data in Table 2, it resulted that $t = 3.5$ minutes is the minimum value for significantly distinguishing the two groups.

The graph shown in Figure 5 allows us to determine the discriminating ability of the test, i.e., how well the test performed can distinguish between positive CA and negative subjects. It gives information on the probability that a randomly extracted subject is correctly classified as CA if positive on the test and as without CA pathology if negative. Accordingly, indices giving AUC values $> .9$ can be considered as very good for discriminating ATTR-CA patients from negative

subjects. From Figure 5 we can see that, for $t > 6$ minutes, both $TAC_{Heart/Bone}(t)$, and $RI_{heart-bone}(t)$, give AUC values $> .9$; moreover, for $t > 10$ minutes the two indices have AUC values very near to the maximum value 1, i.e., Probability = 1 of discriminating of the two groups.

The results herein obtained are consistent with what presented in Galat et al.,¹⁸ where authors analyzed images acquired at 10 minutes from injection and demonstrated that such analysis well predicts late-phase finding.

Dynamic planar images have been acquired from the anterior thorax view. Although the geometric mean between the tracer uptake measured on the anterior and the posterior acquisitions usually allows to obtain more accurate data, in this work we decided to evaluate only the quantitative data obtained on the anterior images because of the preferential bony uptake of the tracer and the consequent high activity of the rib cage which would certainly have introduced more noise reducing the accuracy of the quantification.

As far as the intra- inter-observer variability, it has been chosen to evaluate the variability in two phases of the study, namely in the construction of the TAC curves, which corresponds to the phase that depended more on the operator than all the others, and in determining the time_threshold value, for each index which is determined almost at the end of the analysis. This was done to see how much the variability in ROIs design affected subsequent results.

As it can be seen from Table 3 and the global results obtained, the nRMSE for both the intra- and inter-observer variability is very low, and the SEM values are almost negligible.

From these promising results, we suggest that to have an accurate diagnosis of the presence of CA-ATTR just acquire a single image very early, at about 10 minutes from the injection of the tracer and from this image calculate the Heart/Bone index, after extracting the two corresponding ROIs (i.e., covering the heart and bone

Table 3. nRMSE values obtained from the intra- and inter-observer measurements analysis

ROI	Intra-observer		Inter-observer	
	nRMSE mean (± sd) % controls	nRMSE mean (± sd) % patients	nRMSE mean (± sd) % controls	nRMSE mean (± sd) %patients
Heart	3.16 (0.23)	3.04 (0.24)	6.16 (0.35)	6.23 (0.27)
Bone	2.99 (0.49)	2.92 (0.64)	5.89 (0.55)	6.02 (0.99)
Blood	7.96 (3.09)	3.623 (0.40)	10.59 (3.11)	6.99 (0.49)
Background	2.37 (1.19)	3.34 (0.53)	4.74 (0.90)	6.18 (0.49)

regions). Another solution that we propose is to acquire two or more images in the time interval between 3 and 10 minutes after the injection of the tracer and calculate the retention index of Heart–Bone, after having derived the two ROIs from the acquired images.

Note that, for both indices, the total time of acquisition is very short, greatly reducing waiting times and discomfort for the patient.

Although the number of patients enrolled in this study is not high, the results obtained are still very promising and they can be considered as a suggestion to perform reliable exams, in a short time and at low costs.

NEW KNOWLEDGE GAINED

Early Bisphosphonate (99mTc-HMDP) scintigraphy acquisition and derived indexes analysis can detect ATTR- Cardiac Amyloidosis.

STUDY LIMITATIONS

Our study has limitations. First, the enrolled population is relatively small. However, the proposed approach is a novel dynamic evaluation of cardiac bisphosphonates uptake performed on a population with clinical, biochemical and instrumental characterization of all subjects, including histological demonstration of amyloid deposits. None of our patients had mutations of the gene encoding for transthyretin so these results cannot be extended to patients with hereditary ATTR-CA.

CONCLUSIONS

In this paper, we suggested a method that allows performing CA diagnosis by planar scintigraphy after 99mTc-bisphosphate derivative tracers acquiring early images a few minutes after the tracer administration. A standard Anger gamma-camera is a widespread instrument, available in any nuclear medicine lab. The examination thus proposed allows determining the presence of ATTR-CA, quickly and inexpensively both in terms of examination costs and time spent.

Disclosure

No potential conflict of interest relevant to this article was reported.

References

1. Singh V, Falk R, Di Carli MF, Kijewski M, Rapezzi C, Dorbala S. State-of-the-art radionuclide imaging in cardiac transthyretin amyloidosis. *J Nuclear Cardiol* 2019;26:158-73.

2. Gillmore JD, Maurer MS, Falk RH, Merlini G, Damy T, Dispenzieri A, et al. Nonbiopsy diagnosis of cardiac transthyretin amyloidosis. *Circulation* 2016;133:2404-12.
3. Ansari-Lari MA, Ali SZ. Fine-needle aspiration of abdominal fat pad for amyloid detection: A clinically useful test? *Diagn Cytopathol* 2004;30:178-81.
4. Fine NM, Arruda-Olson AM, Dispenzieri A, Zeldenrust SR, Gertz MA, Kyle RA, Swiecicki PL, Scott CG, Grogan M. Yield of noncardiac biopsy for the diagnosis of transthyretin cardiac amyloidosis. *Am J Cardiol* 2014;113:1723-7.
5. Falk RH, Quarta CC. Echocardiography in cardiac amyloidosis. *Heart Fail Rev* 2015;20:125-31.
6. Cappelli F, Baldasseroni S, Bergesio F, Perlini S, Salinaro F, Padeletti L, et al. Echocardiographic and biohumoral characteristics in patients with AL and ATTR amyloidosis at diagnosis. *Clin Cardiol* 2015;38:69-75.
7. Martinez-Naharro A, Treibel TA, Abdel-Gadir A, Bulluck H, Zumbo G, Knight DS, et al. Magnetic resonance in transthyretin cardiac amyloidosis. *J Am Coll Cardiol* 2017;70:466-77.
8. Fontana M, Chung R, Hawkins PN, Moon JC. Cardiovascular magnetic resonance for amyloidosis. *Heart Fail Rev* 2015;20:133-44.
9. Tang CX, Petersen SE, Sanghvi MM, Lu GM, Zhang LJ. Cardiovascular magnetic resonance imaging for amyloidosis: The state-of-the-art. *Trends Cardiovasc Med* 2019;2:83-94.
10. Pelletier-Galarneau M, Abikhzer G, Giraldeau G, Harel F. Molecular imaging of cardiac amyloidosis. *Curr Cardiol Rep* 2019. <https://doi.org/10.1007/s12350-020-02177>.
11. Genovesi D, Vergaro G, Emdin M, Giorgetti A, Marzullo P. PET-CT evaluation of amyloid systemic involvement with [18F]-florbetaben in patient with proved cardiac amyloidosis: A case report. *J Nucl Cardiol* 2017;24:2025-9.
12. Giorgetti A, Genovesi D, Emdin M. Cardiac amyloidosis: The starched heart. *J. Nucl. Cardiol* 2020;27:133-6.
13. Cappelli F, Gallini C, DiMario C, Costanzo EN, Vaggelli L, Tutino F, et al. Accuracy of 99mTc-hydroxymethylene diphosphonate scintigraphy for diagnosis of transthyretin cardiac amyloidosis. *J Nucl Cardiol* 2019;26:497-504.
14. Andrikopoulou E, Bhambhani P. Nuclear imaging of cardiac amyloidosis. *J Nucl Cardiol* 2019;26:505-8.
15. Bravo PE, Dorbala S. Targeted Nuclear Imaging Probes for Cardiac Amyloidosis. *Curr Cardiol Rep* 2017;19:59.
16. Treglia G, Glaudemans AWJM, Bertagna F, Hazenberg BPC, Erba PA, Giubbini R, et al. Diagnostic accuracy of bone scintigraphy in the assessment of cardiac transthyretin-related amyloidosis: A bivariate meta-analysis. *Eur J Nuclear Med Mol Imaging* 2018;45:1945-55.
17. Ramsay SC, Lindsay K, Fong W, Patford S, Younger J, Atherton J. Tc-HDP quantitative SPECT/CT in transthyretin cardiac amyloid and the development of a reference interval for myocardial uptake in the non-affected population. *Eur J Hybrid Imaging* 2018;2:17.
18. Galat A, Van der Gucht A, Guellich A, Bodez D, Cottereau A, Guendouz S, et al. Early phase 99Tc-HMDP scintigraphy for the diagnosis and typing of cardiac amyloidosis. *JACC* 2017;10:601-3.
19. Chen W, Ton VK, Dilsizian V. Clinical phenotyping of transthyretin cardiac amyloidosis with bone-seeking radiotracers in heart failure with preserved ejection fraction. *Curr Cardiol Rep* 2018;20:23.
20. Perugini E, Guidalotti PL, Salvi F, Cooke RMT, Pettinato C, Riva L, et al. Noninvasive etiologic diagnosis of cardiac amyloidosis using 99mTc-3,3-diphosphono-1,2-propanodicarboxylic acid scintigraphy. *J Am Coll Cardiol* 2005;46:1076-84.

21. Kristen AV, Scherer K, Buss S, Aus Dem Siepen F, Haufe S, Bauer R, et al. Noninvasive risk stratification of patients with transthyretin amyloidosis. *JACC* 2014;7:502-10.
22. Bokhari S, Castano A, Pozniakoff T, Deslisle S, Latif F, Maurer MS. (99m)Tc-pyrophosphate scintigraphy for differentiating light-chain cardiac amyloidosis from the transthyretin-related familial and senile cardiac amyloidoses. *Circ Cardiovasc Imaging* 2013;6:195-201.
23. Gallini C, Tutino F, Martone R, Ciaccio A, Costanzo EN, Taborchi G, et al. Semi-quantitative indices of cardiac uptake in patients with suspected cardiac amyloidosis undergoing 99mTc-HMDP scintigraphy. *J Nucl Cardiol*. 2019 [Epub ahead of print].
24. Gillmore JD, Wechalekar A, Bird J, et al. Guidelines on the diagnosis and investigation of AL amyloidosis. *Br J Haematol* 2015;168:207-18.
25. Antoni G, Lubberink M, Estrada S, Axelsson J, Carlson K, Lindsjö L, et al. In vivo visualization of amyloid deposits in the heart with ¹¹C-PIB and PET. *J Nucl Med* 2013;54:213-20.
26. Law WP, Moore PT, Ng ACT, Wang WYS, Mollee PN. Cardiac amyloid imaging with ¹⁸F-florbetaben PET: A pilot study. *J Nucl Med* 2016;57:1733-9.
27. Popović ZB, Thomas JD. Assessing observer variability: A user's guide. *Cardiovasc Diagn Ther* 2017;7:317-24.
28. Pelletier-Galarneau M, Abikhzer G, Giraldeau G, Harel F. Molecular imaging of cardiac amyloidosis. *Curr Cardiol Rep*. 2019;21:12.
29. Treglia G, Glaudemans AWJM, Bertagna F, Hazenberg BPC, Erba PA, Giubbini R, Ceriani L, Prior JO, Giovannella L, Slart RHJA. Diagnostic accuracy of bone scintigraphy in the assessment of cardiac transthyretin-related amyloidosis: A bivariate meta-analysis. *Eur J Nucl Med Mol Imaging* 2018;45:1945-55.
30. Papantoniou V, Valsamaki P, Kastritis S, Tsiouris S, Delichas Z, Papantoniou Y, et al. Imaging of cardiac amyloidosis by (99m)Tc-PYP scintigraphy. *Hell J Nucl Med* 2015;18:42-50.
31. Castano A, Haq M, Narotsky DL, Goldsmith J, Weinberg RL, Morgenstern R, et al. Multicenter study of planar technetium 99m pyrophosphate cardiac imaging: Predicting survival for patients with AATTR cardiac amyloidosis. *JAMA Cardiol* 2016;1:880-9.
32. Rapezzi C, Quarta CC, Guidalotti PL, Longhi S, Pettinato C, Leone O, et al. Usefulness and limitations of 99mTc-3,3-diphosphono-1,2-propanodicarboxylic acid scintigraphy in the aetiological diagnosis of amyloidotic cardiomyopathy. *Eur J Nucl Med Mol Imaging* 2011;38:470-8.
33. Galat A, Rosso J, Guellich A, Van Der Gucht A, Rappeneau S, Bodez D, et al. Usefulness of (99m)Tc-HMDP scintigraphy for the etiologic diagnosis and prognosis of cardiac amyloidosis. *Amyloid* 2015;22:210-20.

Publisher's Note Springer Nature remains neutral with regard to jurisdictional claims in published maps and institutional affiliations.